Article:

Tomlinson, K., Fletcher, D.I. and Lewis, R. orcid.org/0000-0002-4300-0540 (2022) Evaluation of laser cladding as an in-situ repair method on rail steel. Tribology International. 108210. ISSN 0301-679X

https://doi.org/10.1016/j.triboint.2022.108210

Evaluation of laser cladding as an in-situ repair method on rail steel

K. Tomlinson, D. I. Fletcher, R. Lewis

The University of Sheffield, Department of Mechanical Engineering, Sheffield, UK

Corresponding author: Katherine Tomlinson, kate.tomlinson@sheffield.ac.uk

Abstract

Laser clad coatings have been considered as an in-situ repair method to extend the lifespan of rail. Building on previous research which predominantly focuses on the application of such coatings on full sections of rail this study considers a representative size and geometry of a scaled repair site with the additional consideration of the interface between parent rail and repair at the surface. To enable the evaluation of in-situ repairs a set of experiments were designed to assess multiple repair sites in single tests. Rolling-sliding twin-disc tests were conducted using bespoke rail discs manufactured from standard R260 grade rail steel with six wire eroded slots of varying sizes filled with three different candidate cladding materials, Stellite 6, MSS and R260 powder. The evolution of the surface was monitored through visual observation every 5,000 cycles during the tests, the discs were then sectioned to assess the integrity of the repair and effect of rolling contact loading. During the tests the repair material underwent plastic flow in the direction of traction, experiencing material flow alongside the parent rail steel. The success of laser clad coating as a repair is shown to be dependent on selecting a material which tends to strain by similar amounts to the parent material, making it less vulnerable to crack initiation points forming at the trailing edge where the parent rail may otherwise flow over the repair.

Keywords

Laser cladding, Rail repair, In-situ, Rail-wheel tribology, Rolling contact fatigue

1. Introduction

The lifespan of conventional grades of rail steel is limited by wear and rolling contact fatigue (RCF) which can be costly to repair or replace. The locations of rail which experience high traffic or dynamic loads may be more prone to wear and RCF. They often require repair as an intervention before deformation goes too far, becomes dangerous and requires rail replacement. Such repairs are regularly performed using weld repair, however weld repairs can have their own problems and are susceptible to crack initiation. The initiation and growth of cracks in weld repairs was researched by Jun et al. [1], [2] and Lennart Josefson [3], they both found that residual stress influenced the rate of crack growth. They suggest that the possible causes of failure in weld-repaired rail could be from defects with the weld material like porosity in the weld, lamellar line cracks or a reduction in material hardness, or the changes in microstructure, chemical composition associated with the heat process. Other issues may occur from the thermal process involved in welding or improper pre-heating of the rail. Problems arising from this may include weld breaks, hot tears, porosity and the creation of a heat affected zone.. Additive manufacturing of premium rail materials with higher yield points which are more resistant to plastic damage has been shown in laboratory tests to have the potential to increase the life of rails across the network [4]–[9], as has the application to switch blades in light rail [10]. It is hypothesised that additive manufacturing with laser clad coatings could be utilised as an in-situ method to repair damaged rails as the targeted repair area would experience less impact from the heat process than from a weld repair as the laser is localised and controlled.

The laser clad coating method is at a stage of development where optimised parameters such as pre-heat, laser power and flow rate can be readily achieved by specialist laser cladding operators for full components, however, testing of laser clad coatings for repairs is limited. The Welding Institute (TWI) have reported using a 2 kW CO_2 laser with their 'Trumpf DMD 505 laser deposition system' to create a crack free deposition [11] on full rail components. No pre-heat was applied to the substrate rail, laser power was reportedly 1340 kW, head speed 600 mm/min and powder flow 0.28 g/min. The laser clad process parameters have not yet been optimised for repairs and it has been previously shown that non-optimal parameters can cause porosity, voids or cracks within the coating [12]. The reduced area of the repair and more complex geometry present different challenges, the transition from clad repair to parent rail will create interfaces which could be points of weakness and these are investigated within this study through scaled down tests.

Laser cladding was proposed as a possible method for extending the life of railway wheel surfaces by Niederhauser and Karlsson in 2004 [7] at Chalmers University of Technology, Sweden. This paper references a 1998 patent by Johan Lennart Olofsson [13], however there are no supporting research papers from this inventor at the time. Since then the method for additively manufacturing laser clad coatings to rail steels has been developed, to consider the material choice [4]–[6], [8], [14]–[18], the laser parameters [19] and the effect of thermal processing [3], [18], [20]. Laser cladding was suggested as a potential alternative to weld repairs by Mortzavian [21] and Hernandez [22], there are three papers which report having conducted experiments on laser clad repairs for rail [23]–[25], but none of which have tested the repairs in rolling-sliding conditions experienced in a wheel-rail contact. Seo et al. [23] conducted twin-disc tests with partial cladding specimens using three candidate laser cladding materials, Stellite 21, Hastalloy

C and Inconel 625. They found that the specimens experienced wear at the boundary with dense microstructure due to plastic deformation at the contact surface. Xie et al. [24] also investigated the wear and rolling contact fatigue of laser clad repair sites in twin-disc tests using five different candidate stainless powders 304, 314, 2Cr13, 316L and 434L. The wear rate of the rail was seen to improve, however, fatigue cracks were observed within the clad coating and more severely at the boundary of clad repair and parent rail on both the leading and trailing edge.

Nellian et al. [25] investigated laser clad coatings as a repair method for premium head hardened R350HT grade rail steel. The candidate laser clad coating material chosen was Stellite 6 which was applied to create a strong metallurgical bond at the interface without any porosity or voids present. The heat affected zone was seen to have a higher level of hardness than the clad coating or substrate rail due to the formation of martensite during the laser cladding process. Ball-on-disc tribometer testing was used to observe a reduction in wear of almost 50% in the Stellite 6 coating compared with the unclad rail, although this method does not account for the rolling-sliding conditions experienced in wheel-rail contact.

Within the testing of laser clad coatings by Lewis et al. [5] for the purpose of improving performance of rail, reducing wear and RCF, R260 grade rail steel was used as a clad material. They showed in twin-disc testing that the magnitude and depth of plastic deformation in the clad coating is comparable to the unclad rail disc. They represented a repair of a damaged rail by applying a laser clad R260 grade material onto a R260 grade disc. This was, however, applied as a full complete circumferential coating to test the material itself. This study builds on the success seen with the like for like material but considers the size and geometry of a scaled repair site with the additional consideration of the interface between parent rail and repair at the surface. Further research, however, is required on the RCF behaviour of R260 laser clad coating. It is proposed that if a laser clad repair material and the parent rail tend to strain by similar amounts under load it would be beneficial and is therefore tested as a repair in this paper.

Laser cladding offers a potential method of in-situ application on targeted areas which are more susceptible to damage. It is therefore hypothesised that additive manufacturing with laser clad coatings could be utilised as an in-situ method to repair damaged rails, rather than removing them from track. The targeted repair area would experience less impact from the heat process than from a weld repair as the laser application can be localised and controlled. The results of twin-disc testing with bespoke repaired rail discs presented within this paper provide an assessment of three candidate repair materials. The findings can be used to guide the suitability of in-situ laser clad repairs on rail steels and inform the required mechanical properties required when optimising the laser process parameters.

2. Experimental methodology

2.1. Test apparatus

To enable the evaluation of in-situ repairs, a set of experiments was designed to assess multiple repair sites in single twin-disc tests using bespoke rail discs. Twin-disc testing was conducted on an adapted TE 72 Two Roller Machine made by Phoenix Tribology, now referred to as SUROS 2, which is designed for the study of traction, wear and rolling contact fatigue under pure rolling or rolling-sliding conditions in dry or lubricated conditions, an image of SUROS 2 is shown in Figure 1a.

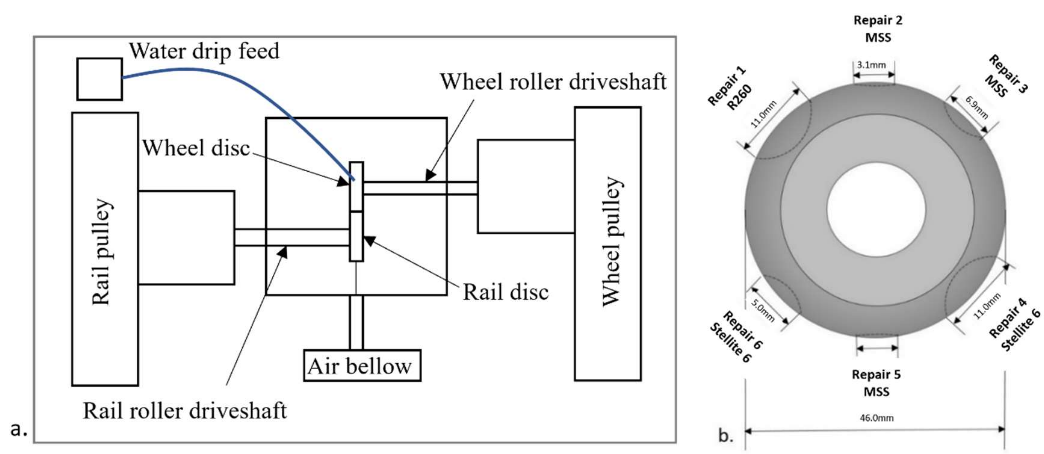

Figure 1: Twin-disc apparatus: a. Aerial schematic of twin-disc test machine; SUROS 2 used to replicate rail-wheel contact in the laboratory. b. Sketch of the repair disc with the repair numbers, materials and width of each repair site.

SUROS 2 has two AC vector motors which are each connected to the test assembly by a timing pulley. The rail and wheel discs are brought into contact and the load is applied horizontally. The connected computer runs the test through the programmed parameters in COMPEND 2000 and slip is created by maintaining a constant speed in the rail disc (approximately 375 rpm) and the wheel disc running at the speed required to generate the programmed slip level, shown in Equation 1.

$$S(\%) = \frac{200(R_r V_r - R_w V_w)}{R_r V_r + R_w V_w}$$

Equation 1

where R_r and R_w are the radii of the rail and wheel disc respectively (mm) and V_r and V_w are the number of revolutions of the rail and wheel discs respectively.

2.2. Test Specimens

The experimental design and results of tests conducted to assess the integrity, surface evolution and rolling contact effect of laser clad repairs are presented here. The rail discs were manufactured from a cylinder of 0.62% carbon steel, representative of R260 commonly found in service across the UK rail network, with six slots wire eroded from the circumference which varied in dimension to assess a combination of shallow, medium and deep repairs. Following previous success in laser clad coating on rail steel, three candidate cladding materials were selected, i) MSS low carbon alloy with 14.64% chromium, ii) R260 grade rail steel with 0.62% carbon steel which is the same as the parent rail steel and iii) Stellite 6 which is cobalt based. The candidate materials were laser clad using the one-step powder injection method described in Lewis et al. [4] with the same optimal parameters used in work by Lewis et al. [5]. The laser process parameters are controlled to avoid the formation of martensite in the HAZ as investigated by Lai et al. [26]. The repair sites are labelled 1 to 6 and the corresponding laser clad material and maximum width of the repair sites are shown in Figure 1b. The test discs have a 47 mm diameter and 10 mm wide running band. The wheel discs were manufactured from ER8 grade steel with ≤0.56 (% by mass) carbon content and a specification of 258-296 HB hardness [27].

An unused sample of material including repairs was sectioned using standard metallographic methods to reveal each individual repair. The repair samples were then etched with 2% Nital (98% Industrial Methylated Spirit (IMS) mixed with 2% nitric acid) to reveal the repair within the parent rail, optical micrographs of each of the repair sites are presented in Figure 2.

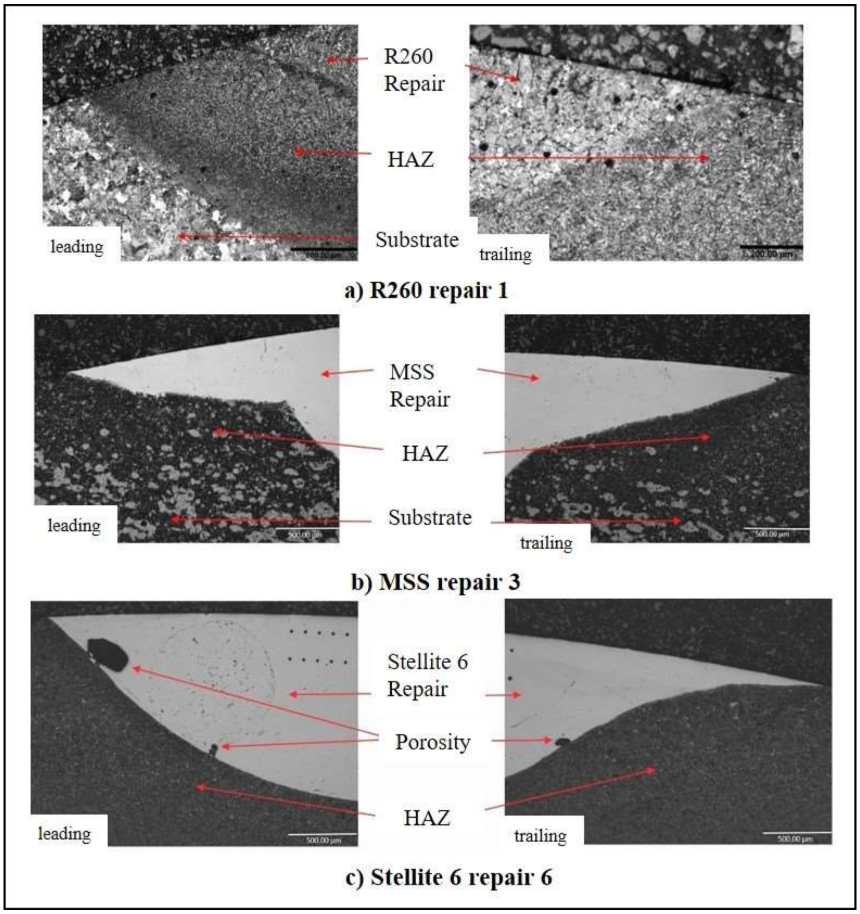

Figure 2: Optical micrographs of the leading and trailing edge of the laser clad repairs, a) R260 repair, b) MSS repair and c) Stellite 6 repair

In repair site 1 (Figure 2a), a fine grain heat affected zone can be seen between the R260 repair and the unaffected substrate rail, it is seen to have a bond of high integrity with no visible flaws at the interface. The MSS repairs (Figure 2b) in sites 2, 3 and 5, appear to have been optimally deposited without inclusions. A small fine grain heat affected zone can be seen between the MSS repair and the unaffected substrate rail. The interfaces of the MSS repair sites to the parent rail are seen to have a good metallurgical bond with mechanical mixing apparent. The Stellite 6 repairs (Figure 2c) in sites 4 and 6 are also seen to have a good metallurgical bond. Large porosity can be seen in the clad repair of repair site 6, indicating the process parameters were not optimal for the Stellite 6 powder. This is due to the process parameters being optimised for larger applications and have not yet been revised for small repair sites which have a smaller area for heat dissipation and hence a faster cooling rate.

The rail disc surface appeared smooth pre-testing and the repairs could not be seen along the running band. Surface observations and measurements were conducted using an optical (non-contact) Alicona PortableRL Infinite Focus microscope. The average surface roughness measurement Ra was 0.36µm across the entire disc. Within the R260 repair area this was slightly higher at 0.41µm, within the MSS repairs it was 0.33µm and within the Stellite 6 repairs it was 0.39µm.

2.3. Test Approach

A system was set up with distilled water, gravity fed through a pipe and clamped over the wheel disc to allow RCF testing in water lubricated conditions to enable investigations into crack initiation and propagation. The rail and wheel disc were both cleaned in an ultrasonic isopropanol bath for 2 minutes before and after testing.

Twin-disc tests were run in dry (unlubricated) conditions with a contact pressure of 1500 MPa at -1% slip, for 30,000 contact cycles, enough to reach steady state wear in the parent R260 grade rail steel [27], [28], to assess the surface evolution of the repairs. Twin-disc tests were also run in a combination of initial dry cycles to generate crack initiation followed by water lubricated conditions to assess RCF crack propagation within the repairs and surrounding material. These were also conducted at 1500MPa, -1% slip with an initial 500 dry cycles to generate deformation within the parent R260 grade rail steel and crack initiation at the surface [29], followed by water lubricated cycles with water dropped onto the wheel disc at a rate of 1 drip per second, to ensure that a film of water was maintained at the contact of the discs given the speed of testing. Table 1 shows the summary of the test plan.

Test	**Dry cycles**	**Water lubricated cycles**	**Water drop rate**	**p_0(MPa)**	**Slip (%)**
Dry	30,000	-	-	1500	-1
RCF short	500	5,000	1 per second	1500	-1
RCF long	500	15,000	1 per second	1500	-1

Table 1: Summary of twin-disc test plan for laser clad repair discs.

The repair sites of laser clad coatings within the rail disc, create points of material interface between the parent rail and clad repair at twelve points per rotation. The novelty of running twin-disc tests with a discontinuous surface material required caution within the RCF tests, as it was assumed that the material interface could provide crack initiation sites. The initial RCF test, therefore, was visually inspected for signs of RCF, in the form of a ‘speckled’ surface or visible material loss, after the first 5,000 wet cycles. The clad R260 repair had some visible RCF speckles and hence the test was stopped to examine this. The test was repeated and extended to generate further RCF in the other repairs as the only visible surface RCF in the first RCF test was in the R260 repair. The second test ran for 500 dry cycles followed by 15,000 wet cycles with water dripped at a rate of one drop per second again. The second test was stopped after 15,000 cycles as the visible material loss had advanced from the level seen in the first test and any further large material loss could have resulted in dynamic loading. The parent R260 grade rail steel would expect to see surface RCF as early as 7,000 cycles [30].

3. Results

3.1. Twin-disc test results: Surface evolution

The surface evolution of each disc was monitored through visual observation every 5,000 cycles. The surface roughness measurements were distorted by wear flakes and material flow at the surface repair interface and it was decided that visual observations provided a more accurate way to monitor the surface evolution. The progress of visual surface observations during the unlubricated tests can be seen in Figure 3a. Material flow at the interface of the repairs and parent rail can be seen from 5,000 cycles. The progress of visual surface observations during the water lubricated tests can be seen in Figure 3b. The appearance of the repair rail disc was smooth after testing with the repair sites visible on the surface.

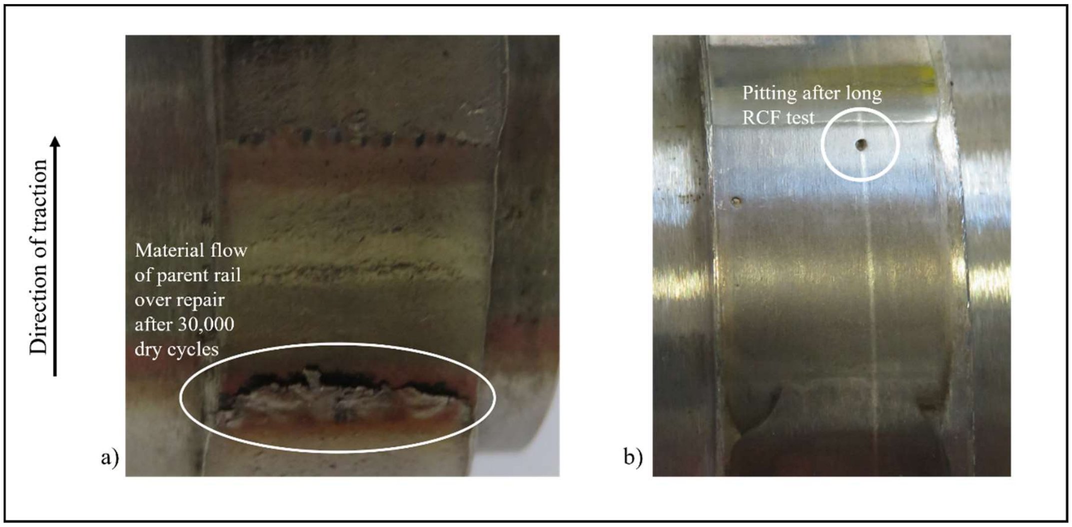

Figure 3: Visual observation of the surface on the repair disc. a) Material flow of parent rail over repair after 30,000 dry cycles and b) Pitting on the surface of a repair after 500 dry cycles and 15,000 water lubricated cycles.

3.1.1. Hardness results

The average hardness of the repairs on the vertical-longitudinal cross section was measured before and after testing using a Durascan micro-hardness tester, with a 0.2 kg load, the results of which are shown in Figure 4. Following testing the rail discs were sectioned and the 6 repairs removed for analysis. The repair sample was prepared using the method described in section 2.2. The pre-test hardness of the R260 clad repair is higher than pre-test R260 grade rail steel and is more in line with a work hardened rail [28]. This is potentially beneficial for a repair which would be applied to servic rail and would provide continuity of hardness at the surface. The hardness of the R260 clad repair reduced slightly after the unlubricated test to 533 Hv0.2 and to an average of 401 Hv0.2 after lubricated RCF testing. This is contrary to the results of the R260 grade rail steel tested in [28] and it appears that R260 applied as a laser clad repair does not work harden and the effective shear yield stress reduces under cyclic loading. It is further expected that the hardness of the R260 pre-testing and after the dry test was inflated due to the inclusion of the transition into the heat affected zone due to the difficulties of identifying the repair location in like for like material, whereas after the water lubricated tests, the repair was easier to locate.

The MSS repairs generally work hardened after cyclic loading, with the exception of repair 3 after the dry unlubricated test. The extent to which the MSS hardened varied between repairs. The small dimensions of repair 2 and repair 5 presented difficulties to taking measurements which were clear of the surrounding parent rail material. The Stellite 6 repairs marginally reduced in hardness after the unlubricated test. After the lubricated RCF tests the hardness increased with the larger repair 4 having the higher increase. The Stellite 6 repairs had the highest hardness of all the candidate repair materials after testing.

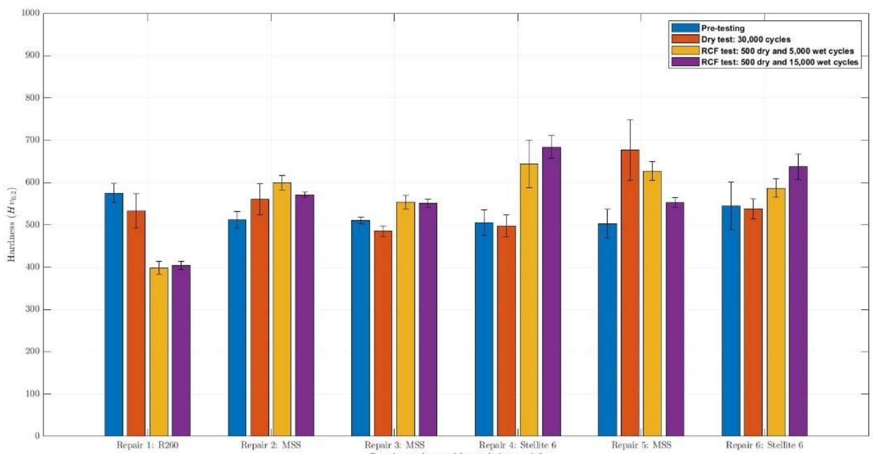

Figure 4: Average hardness and standard deviation of the repairs after each test measured on the longitudinal sub-surface cross-section using micro indentation with a 0.2 kg load.

3.1.2. Unlubricated test results

Following the unlubricated test, the rail disc was sectioned, and the 6 repairs removed for analysis. The repair sample was prepared using the methods described in section 2.2, the vertical-longitudinal cross sections were then observed with optical microscopy. Optical micrographs of R260 repair site 1 are shown in Figure 5 in which material flow at the surface can be seen on the interface with the heat affected zone, and the interface of the heat affect zone and substrate rail on the leading edge. Plastic shear strain was observed down to 140µm below the surface in the middle of the repair site.

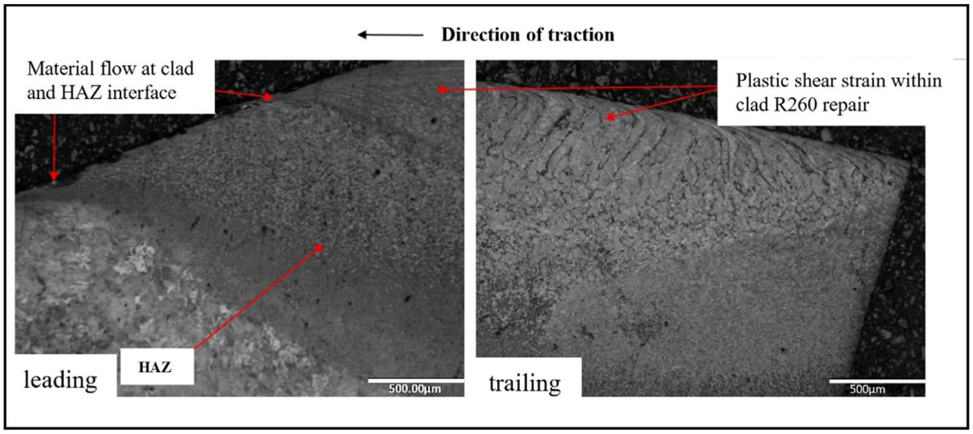

Figure 5: R260 repair 1: Optical micrograph showing material flow in the R260 repair and surrounding heat affected zone.

Optical micrographs of MSS repair 5 are shown in Figure 6. Material flow is observed on the leading edge of MSS repairs, with the clad repair being elongated along the surface and the trailing edge has an area of deformation compared with the untested repair with material swept over in the direction of traction.

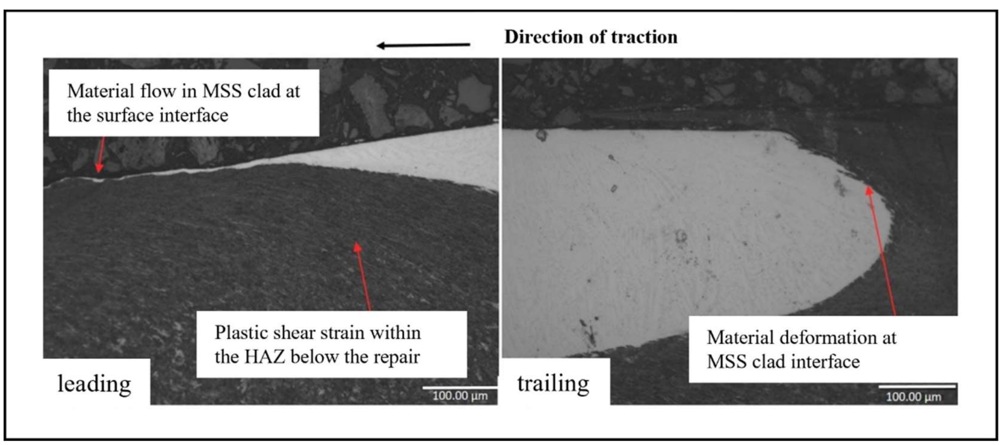

Figure 6: Optical micrographs of MSS Repair 5 after 30,000 unlubricated cycles with material flow in the leading edge of MSS repair and surrounding heat affected zone, and material deformation in the trailing edge.

Optical micrographs of Stellite 6 repair 4 are shown in Figure 7. Repair 4 is a deep repair and material flow is observed on the leading edge, with the clad repair being elongated along the surface and the trailing edge has an area of deformation. There was evidence of material flow in the leading edge of repair 6 and a subsurface crack could be seen at the repair interface of the trailing edge to a depth of around 100 μm, with material swept in the direction of traction.

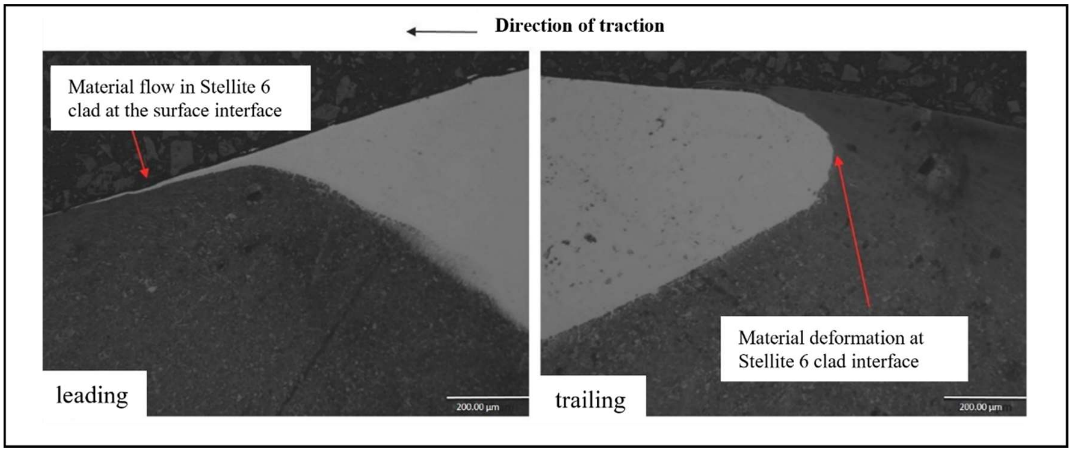

Figure 7: Stellite 6 repair 4 after 30,000 dry cycles. Optical micrograph of material flow in the leading edge and material deformation in the trailing edge.

3.1.3. Water lubricated test results

After both the short and long RCF tests, the surface of the repairs within the discs were imaged using an optical (non-contact) Alicona PortableRL Infinite Focus microscope. The rail disc was again sectioned and the 6 repairs removed for analysis. Figure 8a shows the surface images and optical micrographs of R260 repair 1 after the short RCF test and the below surface RCF damage is apparent. A significant network of cracks can be seen to a depth of 810 μm below the contact surface. The leading edge of the repair (Figure 8b) was intact with no signs of RCF, however material flow at shallow levels was identified, comparable to the unlubricated tested R260 repair. After the long RCF test there were no obvious signs of RCF below the surface and the trailing edge appeared to remain with a strong bond at the interface. The leading edge of the R260 repair had less material flow than the previous tests. It is expected that a small imperfection or inclusion was present at the surface of the repair site in the short RCF test that suffered the excessive RCF crack. This indicates that optimal process parameters would be vital to avoiding initiation of cracks.

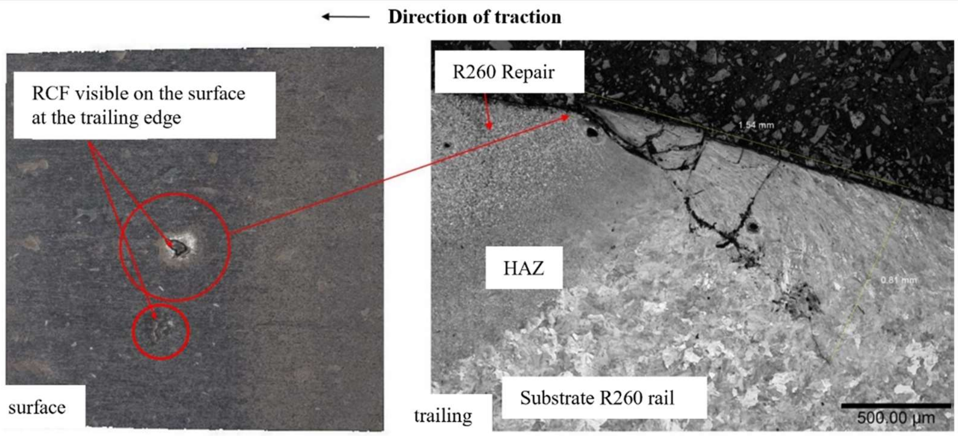

a) R260 Repair 1 after short RCF test: Alicona image showing sign of RCF on the surface and optical micrograph showing network of cracks below the RCF seen on the surface.

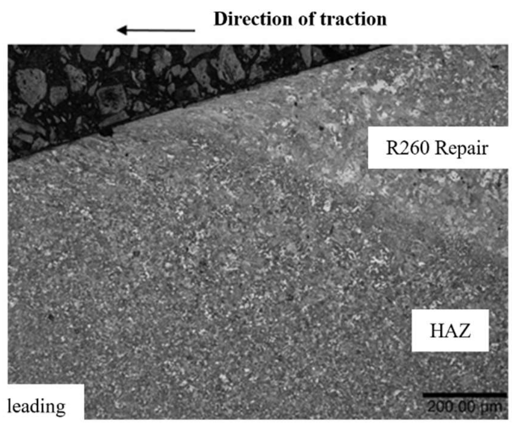

b) R260 Repair 1 after short RCF test: Optical micrograph of the R260 repair leading edge.

Figure 8: R260 Repair 1: a) and b) Following short RCF test of 500 dry cycles followed by 5,000 water lubricated cycles.

The surface images and scanning electron micrographs (SEM) of MSS repairs 3 following the short and long RCF tests are shown in Figure 9. The surface image and SEM micrographs of repair 3 can be seen in Figure 9a following the short RCF test. The trailing edge of repair 3 after the short RCF test can be seen with material flow on the surface and a subsurface RCF crack at the interface resemble those seen in repair 2, yet deeper at around 29 µm below the surface. Similarly, the leading edge is intact with minimal material flow and no signs of RCF as also seen for repair 2. After the long RCF test

(Figure 9b), material flow on the surface interface and a small subsurface RCF crack to a depth of 5 µm below the surface can be observed. A small hollow on the surface of the leading edge can be seen, and a fragment of around 62 µm wide and 26 µm deep of the MSS repair can be seen spalling from the surface after sectioning.

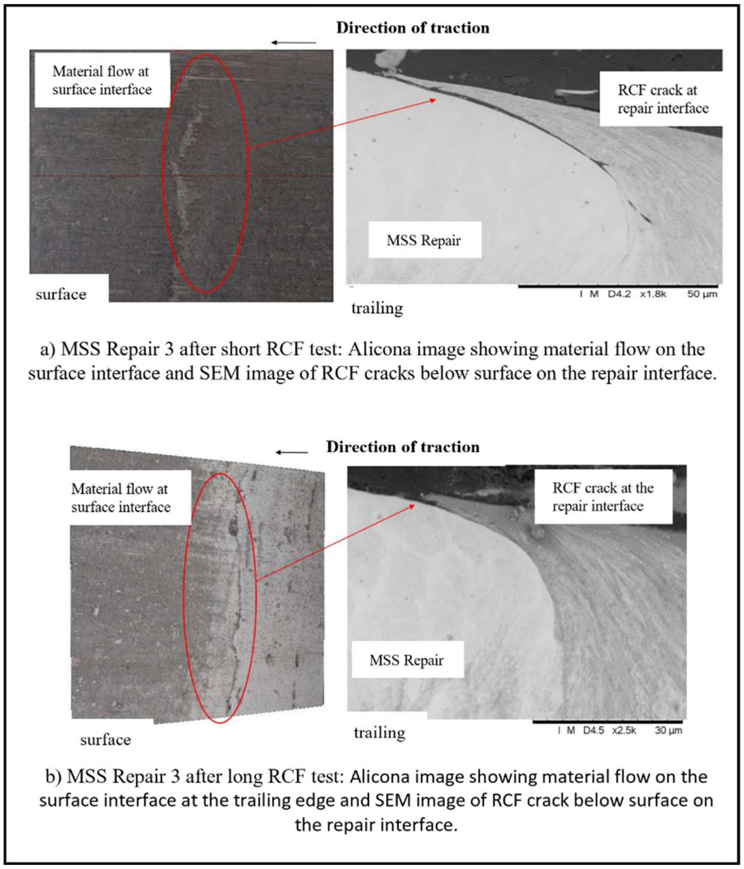

Figure 9: MSS repair 3 following a) short RCF test and b) long RCF tests.

The surface of Stellite 6 repair 4 after the short RCF test can be seen in Figure 10a, with some material flow seen at the interface om the leading edge. When examining the cross section of the trailing edge with SEM, subsurface material deformation and surface damage is observed on the trailing edge of the repair. The leading edge of repair 4 has elongation of the repair at the surface with material flow in the direction of traction. After the long RCF test the surface of the trailing edge of repair 4 has less material flow than in the shorter RCF test, believed to be due to a non-optimal laser parameter defect within the clad of the test specimen in the shorter test.

The leading edge of Stellite 6 repair 6 after the short RCF test is shown in Figure 10b, the interface is seen to be intact with no material flow or RCF evident. Surface damage at the trailing edge of the repair interface of repair 6 can be seen and the SEM image shows subsurface material deformation with material loss shown within the parent R260 rail steel at the interface of the repair. The leading edge of repair 6 has a small amount of material flow at the surface but no signs of RCF at the interface.

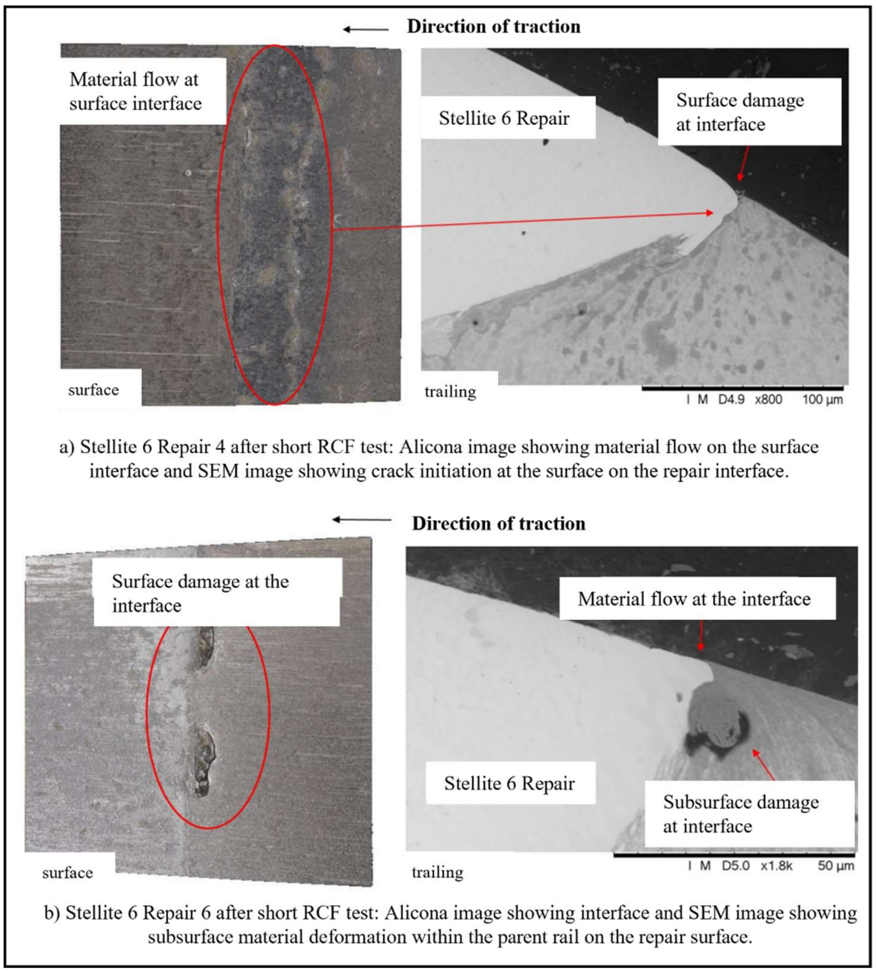

a) Stellite 6 Repair 4 after short RCF test: Alicona image showing material flow on the surface interface and SEM image showing crack initiation at the surface on the repair interface.

b) Stellite 6 Repair 6 after short RCF test: Alicona image showing interface and SEM image showing subsurface material deformation within the parent rail on the repair surface.

Figure 10: Stellite 6 a) repair 4 following short RCF test and b) repair 6 following short RCF test.

4. Discussion

The three candidate materials tested here for the purpose of in-situ laser clad repairs had varying success. The R260 repair had a large heat affected zone and the hardness of the clad R260 was also much higher than standard R260 grade steel. These characteristics are likely to have been as a result of the pre-heat and duration of cooling which is likely to have been faster in a reduced area. The same extent of heat affected zone was observed by Seo et al. [23] in partial clad specimens.
Inclusions or porosity were identified in some of the MSS and Stellite 6 repairs, which is assumed to be caused by the feed rate or head speed of the laser cladding process or the geometry of the repair channel. When sectioned the medium depth MSS repair 3 had evidence of inclusions observed in the sample subjected to the unlubricated test and the sample subjected to the longer RCF test, resulting in material spalling from the surface. The two shallow MSS repairs had no signs of porosity or inclusions, suggesting that the laser process parameters were optimal for a cladding closer to the surface. Both of the Stellite 6 repair sites had inclusions or porosity. After sectioning it was observed that the deep Stellite 6 repair 4 had a large surface cavity and porosity within the repair following the longer RCF test. The medium Stellite 6 repair 6 was seen to have inclusions in the untested repair sample. Following the short RCF test repair 6 was seen to be moving away from the parent rail at the trailing edge and a cavity was seen to be forming at the interface. After the longer RCF test repair 6 had moved away from the parent rail interface and a large subsurface cavity had formed. Inclusions from non-optimal process parameters are assumed to be responsible for this subsurface weakness at the interface. Where inclusions are present within the repair, away from the surface interface, materials tolerated these defects well, with no RCF cracks propagating from them. Further work is to be conducted to assess the tolerance of inclusions within laser clad coatings deposited with imperfect process parameters.

The interface between repair site and parent rail at the trailing edge was the most vulnerable part of the repairs as seen with areas of white etching layer (WEL) [31]. Hiensch et al. [32] found that stop/start section of laser cladding with a coating of different material properties to the substrate caused joins susceptible to crack initiation. The R260 repair had fewest defects at this interface, with the exception of the short RCF test which saw a substantial network of cracks develop. As the R260 repair did not develop any RCF cracks in the longer RCF test further testing is required to understand the level of crack resistance in this type of repair. The cracks on the trailing edge of the Stellite 6 and MSS repairs which are significantly harder than the parent rail are representative of the cracks seen around sites of WEL which is also an area which can have hardness of up to three times higher than the substrate rail [31], [33]–[36].

Plastic shear strain was observed in and below some of the repairs. The R260 repair experienced material flow in the repair, heat affected zone and parent rail as would be expected with the single material region. The material selection for non-continuous laser clad coating applications is seen to be important to the integrity of the repair. The clad material must be perfectly compatible in terms of not only plastic strain accumulation, but also Young's modulus, Poisson's ratio and thermal properties. For a repair this is more important than the extra wear resistant properties, which would actually have a negative effect as the surrounding parent rail wears faster.

The observed elongation of the repair material along the surface and plastic strain accumulation in the heat affected zone below the repair sites echoes that seen in the test in [28] in which a thin layer of MSS was laser clad to the R260 substrate rail and shear strain was accumulated in the heat affected zone. This emphasises the importance of coating or repair depth to ensure the peak stresses occur within the coating. The thin gradient to surface in the deep repair causing a lip of thin laser clad coating is therefore not an optimal design. This is an important result to support the future use of non-continuous laser clad coating application.

5. Conclusions

A series of tests have been designed and conducted to evaluate the integrity, surface evolution and RCF resistance for in-situ laser clad repairs with three candidate materials. The tests were run as standard twin-disc tests with the rail discs being manufactured with 6 repairs around the disc surface. Laser clad coatings applied as an in-situ rail repair is a novel application and this is the first time a small repair has been manufactured and tested under cyclic loading in a scaled test. Laser clad coating process parameters have previously been optimised for larger sections of rail rather than small repair sites. The majority of repairs were clad to a good standard, there were a few that had inclusion or porosity although the repairs tolerated these well. To take the method forward the process parameters including the control of pre heating and cooling must be optimised to avoid porosity within the repair and surrounding rail material.

The R260 clad repair had a greater level of surface modification than the harder clad materials, however, this appeared comparable to standard R260 grade rail steel. The results further indicate that the geometry of the repairs should be carefully designed to avoid a thin lip towards the surface. This could be achieved by optimising the defined pocket shape to be machined out in preparation of the in-situ repair.

RCF cracks were found to most commonly occur on the trailing edge. During the tests the repair material was swept in the direction of traction, driven by the material flow of the parent rail. In many cases where a harder MSS or Stellite 6 repair was present the

R260 grade parent rail swept over the repair site on the surface at the interface. It was below this overlap of material that RCF cracks were most regularly found.

For the purpose of a repair the laser clad coating material that appears to be the most promising is the R260. Being an identical material to the parent rail it has a comparable rate of plastic shear strain accumulation and is therefore less vulnerable to crack initiation points forming at the trailing edge where the parent rail may otherwise flow over the repair. Following the observation of the shallow repairs experiencing plastic strain accumulation within the heat affected zone and the subsequent elongation of laser clad repair along the surface, it is concluded that the depth of laser clad coating is important in its success.

Declaration of Conflicting Interests

The author(s) declared no potential conflicts of interest with respect to the research, authorship, and/or publication of this article.

Funding

The author(s) disclosed receipt of the following financial support for the research, authorship, and/or publication of this article: This project is funded through Industrial Case (Cooperative Awards in Science and Technology) studentship number 17100018 with the EPSRC (Engineering and Physical Sciences Research Council) National Productivity Fund and Network Rail Infrastructure Limited. For the purpose of open access, the author has applied a Creative Commons Attribution (CC BY) license to any Author Accepted Manuscript version arising.

References

[1] H. K. Jun, J. W. Seo, I. S. Jeon, S. H. Lee, and Y. S. Chang, ‘Fracture and fatigue crack growth analyses on a weld-repaired railway rail’, *Engineering Failure Analysis*, vol. 59, pp. 478–492, 2016, doi: 10.1016/j.engfailanal.2015.11.014.

[2] H.-K. Jun, D.-W. Kim, I.-S. Jeon, S.-H. Lee, and Y.-S. Chang, ‘Investigation of residual stresses in a repair-welded rail head considering solid-state phase transformation’, *Fatigue and Fracture of Engineering Materials and Structures*, vol. 40, pp. 1059–1071, 2017, doi: 10.1111/ffe.12564.

[3] B. L. Josefson and J. W. Ringsberg, ‘Assessment of uncertainties in life prediction of fatigue crack initiation and propagation in welded rails’, *International Journal of Fatigue*, vol. 31, no. 8–9, pp. 1413–1421, 2009, doi: 10.1016/j.ijfatigue.2009.03.024.

[4] S. R. Lewis, R. Lewis, and D. I. Fletcher, ‘Assessment of laser cladding as an option for repairing/enhancing rails’, *Wear*, vol. 330–331, pp. 581–591, 2015, doi: 10.1016/j.wear.2015.02.027.

[5] S. R. Lewis *et al.*, ‘Improving rail wear and RCF performance using laser cladding’, *Wear*, vol. 366–367, pp. 268–278, 2016, doi: 10.1016/j.wear.2016.05.011.

[6] S. R. Lewis *et al.*, ‘Full-scale testing of laser clad railway track; Case study – Testing for wear, bend fatigue and insulated block joint lipping integrity’, *Wear*, vol. 376–377, pp. 1930–1937, 2017, doi: 10.1016/j.wear.2017.02.023.

[7] S. Niederhauser and B. Karlsson, ‘Fatigue behaviour of Co-Cr laser cladded steel plates for railway applications’, in *Wear*, 2005. doi: 10.1016/j.wear.2004.03.026.

[8] H. ming Guo, Q. Wang, W. jian Wang, J. Guo, Q. yue Liu, and M. hao Zhu, ‘Investigation on wear and damage performance of laser cladding Co-based alloy on single wheel or rail material’, *Wear*, 2015, doi: 10.1016/j.wear.2015.03.002.

[9] Q. Lai *et al.*, ‘Investigation of a novel functionally graded material for the repair of premium hypereutectoid rails using laser cladding technology’, *Composites Part B: Engineering*, vol. 130, pp. 174–191, 2017, doi: 10.1016/J.COMPOSITESB.2017.07.089.

[10] P. Fasihi, R. Abrahams, P. Mutton, C. Qiu, and W. Yan, ‘Using laser cladding to improve tribological properties of light rails for maintenance’, presented at the 12th International Conference on Contact Mechanics and Wear of Rail/Wheel Systems (CM2022), Melbourne, Australia, 2022.

[11] T. W. Institute, ‘The Cladding of Rail Sections’, 2019.

[12] K. Yildirimli, K. Tomlinson, D. Fletcher, and R. Lewis, ‘Small-scale testing of rail laser cladding longevity , parameter tolerance and in-situ repairs in preparation for field implemetation’, presented at the 12th International Conference on Contact Mechanics and Wear of Rail/Wheel Systems, Melbourne, Australia, 2022.

[13] J. L. Olofsson, ‘Patent: Method for improving the properties of railway wheels’, 1998

[14] A. Clare, O. Oyelola, J. Folkes, and P. Farayibi, ‘Laser cladding for railway repair and preventative maintenance’, *Journal of Laser Applications*, vol. 24, no. 3, pp. 032004–032004, Aug. 2012, doi: 10.2351/1.4710578.

[15] A. T. Clare, O. Oyelola, T. E. Abioye, and P. K. Farayibi, ‘Laser cladding of rail steel with Co–Cr’, *Surface Engineering*, vol. 29, no. 10, pp. 731–736, Nov. 2013, doi: 10.1179/1743294412Y.0000000075.

[16] W. J. Wang, J. Hu, J. Guo, Q. Y. Liu, and M. H. Zhu, ‘Effect of laser cladding on wear and damage behaviors of heavy-haul wheel/rail materials’, *Wear*, 2014, doi: 10.1016/j.wear.2014.01.011.

[17] W. J. Wang, Z. K. Fu, X. Cao, J. Guo, Q. Y. Liu, and M. H. Zhu, ‘The role of lanthanum oxide on wear and contact fatigue damage resistance of laser cladding

Fe-based alloy coating under oil lubrication condition', *Tribology International*, 2016, doi: 10.1016/j.triboint.2015.10.017.

[18] Z. K. Fu, H. H. Ding, W. J. Wang, Q. Y. Liu, J. Guo, and M. H. Zhu, 'Investigation on microstructure and wear characteristic of laser cladding Fe-based alloy on wheel/rail materials', *Wear*, vol. 330–331, pp. 592–599, May 2015, doi: 10.1016/j.wear.2015.02.053.

[19] A. A. Siddiqui and A. K. Dubey, 'Recent trends in laser cladding and surface alloying', *Optics and Laser Technology*, vol. 134, pp. 106619–106619, Feb. 2021, doi: 10.1016/j.optlastec.2020.106619.

[20] S. Niederhauser and B. Karlsson, 'Mechanical properties of laser cladded steel', *Material Science and Technology*, vol. 19, 2003.

[21] E. Mortazavian, Z. Wang, and H. Teng, 'Repair of light rail track through restoration of the worn part of the railhead using submerged arc welding process', *International Journal of Advanced Manufacturing Technology*, vol. 107, no. 7–8, pp. 3315–3332, 2020, doi: 10.1007/s00170-020-05208-x.

[22] F. C. Robles Hernández, A. O. Okonkwo, V. Kadekar, T. Metz, and N. Badi, 'Laser cladding: The alternative for field thermite welds life extension', *Materials and Design*, vol. 111, pp. 165–173, Dec. 2016, doi: 10.1016/j.matdes.2016.08.061.

[23] J. W. Seo, J. –C Kim, S. J. Kwon, and H. K. Jun, 'Effects of Laser Cladding for Repairing and Improving Wear of Rails', *International Journal of Precision Engineering and Manufacturing*, vol. 20, no. 7, pp. 1207–1217, 2019, doi: 10.1007/s12541-019-00115-y.

[24] T. Xie *et al.*, 'Investigation on the Rolling Contact Fatigue Behaviors of Different Laser Cladding Materials on the Damaged Rail', *Journal of Tribology*, vol. 143, pp. 51108–51109, 2021, doi: 10.1115/1.4050690.

[25] A. S. Nellian, K. E. Tan, H. J. Hoh, J. H. L. Pang, I. Christian, and S. Y. Chua, 'Microstructure and Wear Performance Assessment of Laser Cladded Rail Steel for Service Life Extension at Sharp-Radius Curves', in *2018 International Conference on Intelligent Rail Transportation, ICIRT 2018*, Feb. 2019. doi: 10.1109/ICIRT.2018.8641613.

[26] Q. Lai *et al.*, 'Influences of depositing materials, processing parameters and heating conditions on material characteristics of laser-cladded hypereutectoid rails', *Journal of Materials Processing Technology*, vol. 263, pp. 1–20, 2019, doi: 10.1016/j.jmatprotec.2018.07.035.

[27] P. Lu, S. R. Lewis, S. Fretwell-Smith, D. L. Engelberg, D. I. Fletcher, and R. Lewis, 'Laser cladding of rail; the effects of depositing material on lower rail grades', *Wear*, vol. 438–439, 2019, doi: 10.1016/j.wear.2019.203045.

[28] K. Tomlinson, D. Fletcher, and R. Lewis, 'Measuring material plastic response to cyclic loading in modern rail steels from a minimal number of twin-disc tests':, 2021, doi: 10.1177/0954409721993615.

[29] W. R. Tyfour, J. H. Beynon, and A. Kapoor, ‘Deterioration of rolling contact fatigue life of pearlitic rail steel due to dry-wet rolling-sliding line contact’, *Wear*, vol. 197, no. 1–2, pp. 255–265, 1996, doi: 10.1016/0043-1648(96)06978-5.
[30] D. I. Fletcher, F. J. Franklin, and A. Kapoor, ‘Image analysis to reveal crack development using a computer simulation of wear and rolling contact fatigue.’, *Fatigue and Fracture of Engineering Materials and Structures*, vol. 26, pp. 957–967, 2003, doi: 10.1046/j.1460-2695.2003.00696.x.
[31] Q. Lian *et al.*, ‘Crack propagation behavior in white etching layer on rail steel surface’, *Engineering Failure Analysis*, vol. 104, pp. 816–829, 2019, doi: 10.1016/J.ENGFAILANAL.2019.06.067.
[32] E. J. M. Hiensch, F. J. Franklin, and J. C. O. Nielsen, ‘Prevention of RCF damage in curved track through development of the Infra-star two-material rail’, *Fatigue and Fracture of engineering materials and structures*, vol. 26, 2003.
[33] L. Xin, V. Markine, and I. Shevtsov, ‘Analysis of the effect of repair welding/grinding on the performance of railway crossings using field measurements and finite element modeling’, *Proceedings of the Institution of Mechanical Engineers, Part F: Journal of Rail and Rapid Transit*, vol. 232, no. 3, pp. 798–815, 2018, doi: 10.1177/0954409717693960.
[34] R. I. Carroll and J. H. Beynon, ‘Rolling contact fatigue of white etching layer: Part 1. Crack morphology’, *Wear*, vol. 262, no. 9–10, pp. 1253–1266, 2007, doi: 10.1016/j.wear.2007.01.003.
[35] O. Vargolici *et al.*, ‘Influence of the initial surface state of bodies in contact on the formation of white etching layers under dry sliding conditions’, *Wear*, vol. 366–367, pp. 209–216, 2016, doi: 10.1016/j.wear.2016.06.023.
[36] A. Al-Juboori *et al.*, ‘Squat formation and the occurrence of two distinct classes of white etching layer on the surface of rail steel’, *International Journal of Fatigue*, vol. 104, pp. 52–60, 2017, doi: 10.1016/j.ijfatigue.2017.07.005.